PHOTONICS Research

Switchable dual-wavelength Q-switched fiber laser using multilayer black phosphorus as a saturable absorber

Junmin Liu,[1,2,†] Yu Chen,[2,†] Ying Li,[2] Han Zhang,[2] Shuiqin Zheng,[1,2] and Shixiang Xu[1,*]

[1]Shenzhen Key Laboratory of Micro-Nano Photonic Information Technology, College of Electronic Science and Technology, Shenzhen University, Shenzhen 518060, China
[2]International Collaborative Laboratory of 2D Materials for Optoelectronics Science and Technology, Key Laboratory of Optoelectronic Devices and Systems of Ministry of Education and Guangdong Province, College of Optoelectronic Engineering, Shenzhen University, Shenzhen 518060, China
*Corresponding author: shxxu@szu.edu.cn

Received 20 November 2017; revised 16 January 2018; accepted 17 January 2018; posted 17 January 2018 (Doc. ID 313670); published 27 February 2018

Black phosphorus (BP), with thickness-dependent direct energy bandgaps (0.3–2 eV), shows an enhanced nonlinear optical response at near- and mid-infrared wavelengths. In this paper, we present experimentally multilayer BP flakes coated on microfiber (BCM) as a saturable absorber with a modulation depth of 16% and a saturable intensity of 6.8 MW/cm^2. After inserting BCM into an Er-doped fiber ring laser, a stable dual-wavelength *Q*-switched state with central wavelengths of 1542.4 nm and 1543.2 nm (with wavelength spacing as small as 0.8 nm) is obtained with the aid of two cascaded fiber Bragg gratings as a coarse wavelength selector. Moreover, single-wavelength *Q*-switched operation at 1542.4 nm or 1543.2 nm is also realized, which can be switched between the two wavelengths flexibly just by adjusting the intracavity birefringence. These results suggest that BP combined with the cascaded fiber gratings can provide a simple and feasible candidate for a multiwavelength fiber laser. Our fiber laser may have potential applications in terahertz generation, laser radar, and so on.

OCIS codes: (140.3510) Lasers, fiber; (140.4050) Mode-locked lasers; (160.4330) Nonlinear optical materials; (190.7110) Ultrafast nonlinear optics.

https://doi.org/10.1364/PRJ.6.000198

1. INTRODUCTION

Multiwavelength fiber lasers, particularly switchable multiwavelength fiber lasers, have widespread applications in environmental sensing, optical communication, and microwave radiation [1–5]. However, the homogeneous gain broadening can not only cause inherent instability, but also enlarge the wavelength spacing (usually greater than 1 nm) of their emitting pulses [6,7], which makes it difficult to achieve stable multiwavelength pulse operation. Many efforts have been devoted to stabilizing and narrowing the wavelength spacing of multiwavelength fiber lasers, such as via inhomogeneous loss mechanisms [8], the polarization hole burning effect [9], cooling Er-doped fiber (EDF) in liquid nitrogen [10], and the four-wave mixing (FWM) effect [11]. On the other hand, miniaturization and integration of pulsed lasers have also drawn lots of attention. Inserting a saturable absorber (SA) is one of the most effective methods of achieving a compact pulsed laser. As is known, saturable absorption is mainly determined by the imaginary part, while the FWM effect is dominated by the real part, of the third-order optical nonlinearity. Therefore, an SA with high third-order optical nonlinearity is preferred to obtain a stable multiwavelength pulsed fiber laser with a small wavelength space [12].

Recently, it is no exaggeration to say that two-dimensional (2D) materials, particularly graphene, have triggered a flood of interest in the field of all-optical devices, ultrafast lasers, and optical communication, etc., due to their excellent nonlinear optical properties [13,14]. Some experimental results show that both graphene and topological insulators exhibit broadband saturable absorption at 800 nm [15], 1064 nm [16], and 1550 nm [17], and even at terahertz spectral region [18]. Their applications for multiwavelength pulsed-laser generation (*Q*-switched/mode locking) have been extensively studied [19–25]. Moreover, graphene has a giant nonlinear refractive index of $n_2 \sim 10^{-7}$ cm$^2 \cdot$ W^{-1}, almost nine orders of magnitude larger than that of bulk dielectrics [26], and topological

insulators also reach 10^{-14} $m^2 \cdot W^{-1}$ [27], which may cause a strong FWM effect and suppress mode competing, thus improve the stability of a multiwavelength laser. By using a 2D-material-based SA, a stable multiwavelength, single-longitudinal-mode fiber laser can be achieved [28,29]. All these factors predict the potential applications of 2D materials in the field of multiwavelength fiber lasers.

Unfortunately, the absence of bandgap and the low damage threshold dramatically hamper applications where strong light–matter interaction and special operating wavelength are required [5,19]. Recently, another rising 2D material, black phosphorus (BP), has attracted researchers' efforts. As with graphite, van der Waals interactions allow layers of phosphorene to be stacked, and its direct bandgap can be tuned from 2 eV (bulk) to 0.3 eV (monolayer) by controlling its layers, covering almost the whole band of IR and mid-IR [30,31]. The proper "gap" can effectively enhance the nonlinear absorption at a special wavelength. Some reports have also confirmed that multilayer BP has excellent nonlinear absorption characteristics and a strong FWM effect at IR and mid-IR wavelengths [32–35]. However, under high-power laser irradiation, BP can be chemically modified quite easily, which will deteriorate its optical properties and prevent its use in high-power lasers [36].

This paper presents experimentally a stable switchable dual-wavelength erbium-doped *Q*-switched fiber laser obtained by using a BP-based SA. Here, multilayer BP flakes are coated on a microfiber to fabricate an SA using the optical deposition method. As the light interaction with BP is implemented via long-distance evanescent waves, this device can guarantee the saturable absorption characteristic and enhance the FWM effect and tolerance for high-optical-power illumination. In our laser cavity, two cascaded fiber Bragg gratings with a wavelength spacing as small as 0.8 nm are used as a coarse wavelength selector, while a BP-based SA is used to realize *Q*-switched operation. As a result, stable dual-wavelength *Q*-switched laser pulse operation has been obtained with central wavelengths of 1542.4 nm and 1543.2 nm. Furthermore, by carefully adjusting the polarization controller (PC), single-wavelength *Q*-switched operation either at 1542.5 nm or at 1543.2 nm is also achieved, which can be flexibly switched between the two wavelengths.

2. CHARACTERIZATIONS OF THE BP SA AND EXPERIMENTAL SETUP

In the experiment, a liquid phase exfoliation method is used to fabricate multilayer BP flakes with an average thickness of about 15–20 nm (a single layer of BP has a thickness of ~0.6 nm) [37]. As shown in Fig. 1(a), a single-mode fiber (SMF) is tapered to about 24 mm in length and 9 μm in diameter using an oxyhydrogen flame. Through optical deposition, the prepared BP flakes are then deposited on the polished side of the tapered fiber to fabricate a BP flakes coated microfiber (BCM) device. Figure 1(b) shows an optical image of the tapered fiber after deposition; as can be seen, BP flakes were well dispersed over the polished side of the tapered fiber. A balanced twin-detector measurement device, as shown in Fig. 1(c), is aligned to characterize the nonlinear optical property of the BCM. Here, a 6.025 MHz, 1.8 ps, 1550 nm fiber laser is used as a light source. As shown in Fig. 1(d), this BCM device has obvious nonlinear saturable behavior with a modulation depth of 16% and saturation intensity of 6.8 MW/cm^2. The total insertion loss of the BCM was measured at about 1.57 dB.

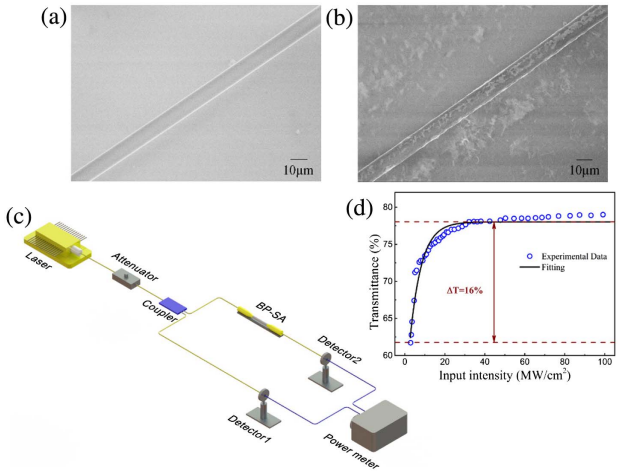

Fig. 1. Optical images of (a) bare microfiber and (b) microfiber coated with BP flakes, (c) experimental setup of the balanced twin-detector measurement device, (d) the measured saturable absorption and its corresponding fitting curve.

The proposed switchable dual-wavelength *Q*-switched fiber ring laser is schematically shown in Fig. 2 with a total cavity length of about 12 m. A 1-m-long highly doped fiber (EDF, LIEKKI Er80-8/125) is used as a gain medium. All the other fibers are standard SMF. The EDF was pumped by a 975 nm laser diode coupled by a 980/1550 wavelength division multiplexer (WDM) coupler. Two fiber Bragg gratings with central wavelengths of 1542.4 nm and 1543.2 nm are cascaded as a coarse wavelength selector, and a PC is employed to adjust the intracavity birefringence. The unidirectional operation of the fiber laser is ensured by a circulator. A 70:30 fiber coupler is used so that 30% of the laser power outputs from the laser cavity, while the rest works as feedback inside the cavity.

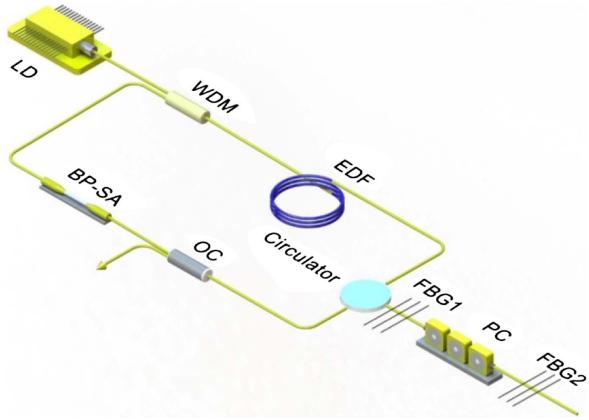

Fig. 2. Schematic of the BP-based *Q*-switched fiber ring laser. LD, laser diode; WDM, wavelength division multiplexer; OC, optical coupler; EDF, Er-doped fiber; FBG, fiber Bragg grating; PC, polarization controller.

Between the fiber coupler and the WDM, the prepared BCM is introduced as an SA. The laser output is monitored with an optical spectrum analyzer (Ando AQ-6317B), a 500 MHz oscilloscope (Tektronix TDS3054B), a 5 GHz photodetector, and a 7 GHz electrical spectral analyzer simultaneously.

3. RESULTS AND DISCUSSION

A. BP-Based Dual-Wavelength *Q*-Switched Pulse Laser

Once the pump power increases to 55 mW, the self-started *Q*-switched state occurs. Dual-wavelength *Q*-switched outputs at a pump power of 95 mW are shown in Fig. 3. In Fig. 3(a) we can see that the output dual wavelengths are located at 1542.4 nm and 1543.2 nm, with a spacing as small as 0.8 nm. Figure 3(b) shows the dual-wavelength *Q*-switched pulse train, which has a repetition rate of 8.19 kHz, corresponding to a time interval of 122 μs. From the profile of the single pulse in Fig. 3(c), we can see that the output pulses have a full width at half-maximum of 17.92 μs, with a symmetric temporal profile. Also, we have measured the corresponding radio frequency (RF) spectrum, with a resolution bandwidth of 10 Hz. As shown in Fig. 3(d), the central frequency is 8.13 kHz, which agrees with the pulse repetition rate very well. The signal-to-noise ratio (SNR) is over 40 dB, indicating the high stability of the laser output. Figure 4 shows the evolution of the dual-wavelength *Q*-switched pulse performance as the pump power increases from 55 to 140 mW with the PC unchanged. As noted in Fig. 4(a), the average output power and the pulse energy increase from 0.5 to 2.3 mW and from 5 to 140 nJ with the pump power, respectively. Once the pump power exceeds 140 mW, the *Q*-switched operation becomes unstable. Further increasing the pump power will result in the replacement of the *Q*-switched state continuous-wave operation, but it can be recovered just by decreasing the pump power again. Figure 4(b) shows the evolution of the repetition rate and pulse width with pump power. When the repetition rate of the *Q*-switched pulses increases from 5 to 13 kHz, the pulse duration decreases from 45 to 5 μs consistently. To investigate the stability of the dual-wavelength *Q*-switched pulse output, we have recorded the lasing spectra at 10 min intervals over 1 h at room temperature. As shown in Fig. 5, the spectra present high long-term stability; neither wavelength shift nor jitter is apparent during our measurements.

To further characterize the *Q*-switched pulse trains at each wavelength from the dual-wavelength laser, a tunable narrow bandpass filter is used to choose the output wavelength. Also at a pump power of 95 mW, Figs. 6 and 7 present the measured output spectra, pulse trains, and radio-frequency spectra of each wavelength (at 1542.4 and 1543.2 nm,

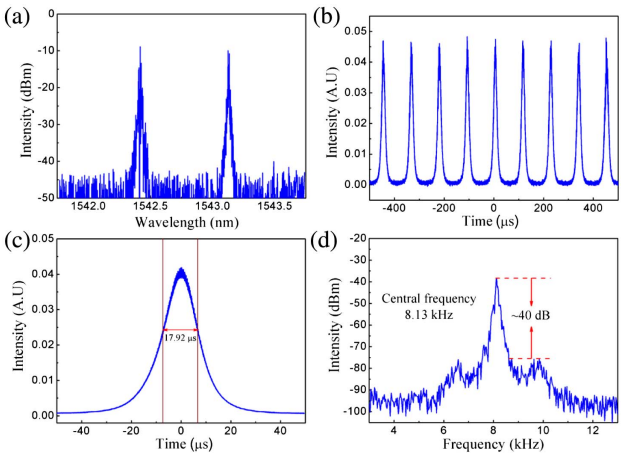

Fig. 3. Dual-wavelength *Q*-switched operation when the pump power is 95 mW. (a) Output optical spectrum of the dual-wavelength *Q*-switched fiber laser, (b) typical *Q*-switched pulse train, (c) single pulse envelope, (d) the RF spectrum.

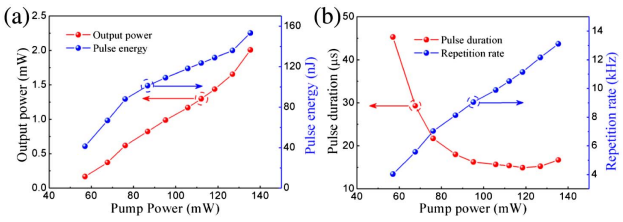

Fig. 4. (a) Average output power and pulse energy versus pump power, (b) the pulse repetition rate and duration versus pump power.

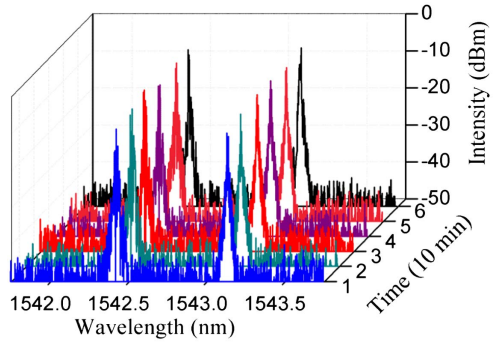

Fig. 5. Output spectra of dual-wavelength *Q*-switched operation taken at a 10 min interval over 1 h.

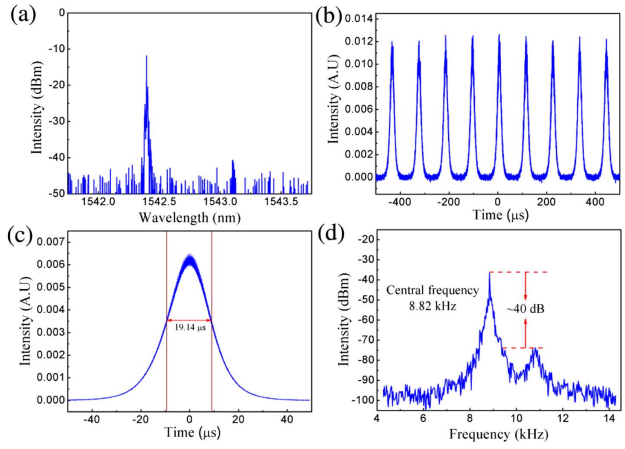

Fig. 6. *Q*-switched operation at a wavelength of 1542.4 nm filtered from dual-wavelength output. (a) Output optical spectrum, (b) typical *Q*-switched pulse train, (c) single pulse envelope, (d) the RF spectrum.

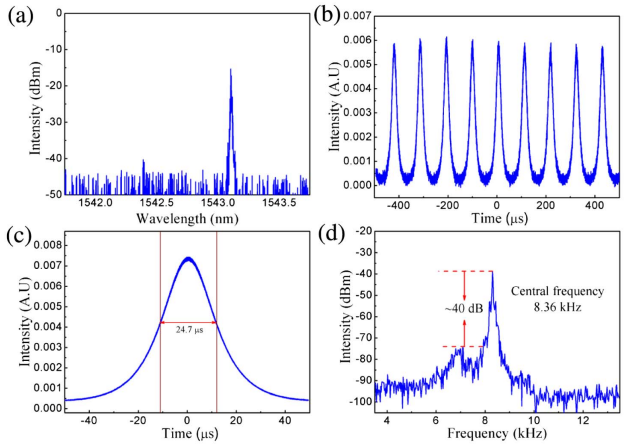

Fig. 7. *Q*-switched operation at a wavelength of 1543.2 nm filtered from dual-wavelength output. (a) Output optical spectrum, (b) typical *Q*-switched pulse train, (c) single pulse envelope, (d) the RF spectrum.

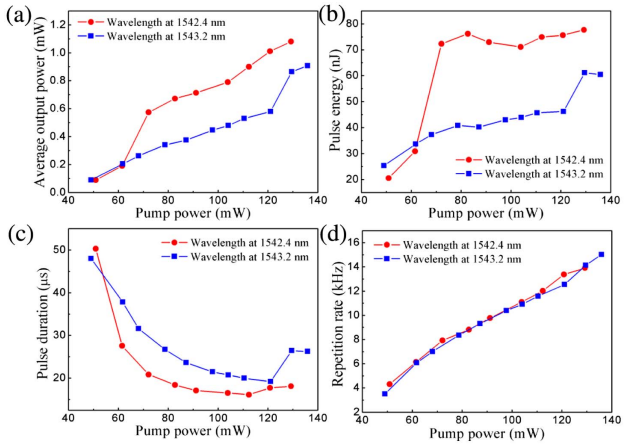

Fig. 8. Dual-wavelength *Q*-switched operation. (a) The average output power, (b) pulse energy, (c) pulse duration, and (d) repetition rate at the wavelengths 1542.4 nm and 1543.2 nm versus pump power.

respectively). We can see that the pulse duration can be estimated to be about 19.14 or 24.7 μs, while the repetition rate is about 8.82 or 8.36 kHz at 1542.4 or 1543.2 nm, respectively. The SNRs of the two wavelengths are both over 40 dB. To compare the pulse performance of these two wavelengths, we increase the pump power from 50 to 140 mW while keeping the other conditions unchanged. As shown in Fig. 8(a), the average output power increases from 0.1 to 1.1 mW at 1542.4 nm, and it increases from 0.1 to 0.9 mW at 1543.2 nm. As seen in Fig. 8(c), the pulse duration decreases from 51 to 10 μs at 1542.4 nm, and from 49 to 18 μs at 1543.2 nm. The duration at 1543.2 nm is little larger than that at 1542.4 nm, which can be attributed to the different cavity lengths. However, the repetition rates of the two wavelengths are pretty much the same, as shown in Fig. 8(d), which explains why no obvious walk-off between the pulse trains of the dual-wavelength operation is observed.

B. BP-Based Single-Wavelength *Q*-Switched Pulse Laser

By adjusting the PC, thereby causing the cavity birefringence to form an equivalence filter, the output spectra can be flexibly switched between 1542.4 nm and 1543.2 nm, as shown in Figs. 9(a) and 10(a), at a pump power of 95 mW. Figures 9(b) and 10(b) show that the pulse train typically has a repetition rate of about 8.62 kHz at 1542.4 nm or 6.36 kHz at 1543.2 nm. In addition, Figs. 9(c) and 10(c) present the real-time recorded single pulse profile with a pulse duration of 12.02 μs at 1542.4 nm and 16.54 μs at 1543.2 nm. The corresponding RF spectrum at 1542.4 nm with a central frequency of 8.62 kHz is shown in Fig. 9(d), while that at 1543.2 nm with a central frequency of 6.36 kHz is shown in Fig. 10(d). It is worth noting that both single-wavelength operations have a relatively high SNR of 45 dB, suggesting that they operate with high stability.

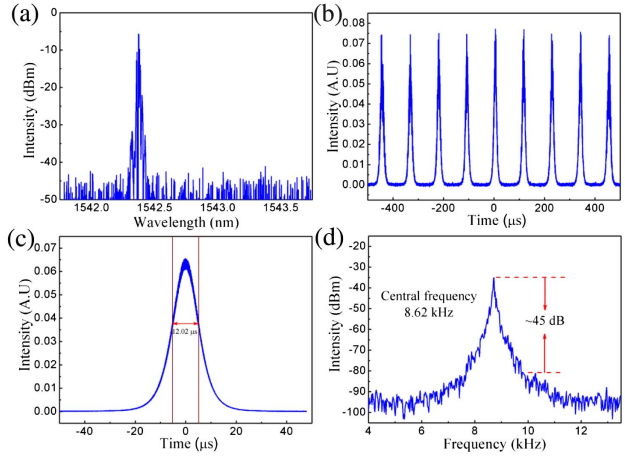

Fig. 9. *Q*-switched operation at a single wavelength of 1542.4 nm. (a) Output optical spectrum, (b) typical *Q*-switched pulse train, (c) single pulse envelope, (d) the RF spectrum.

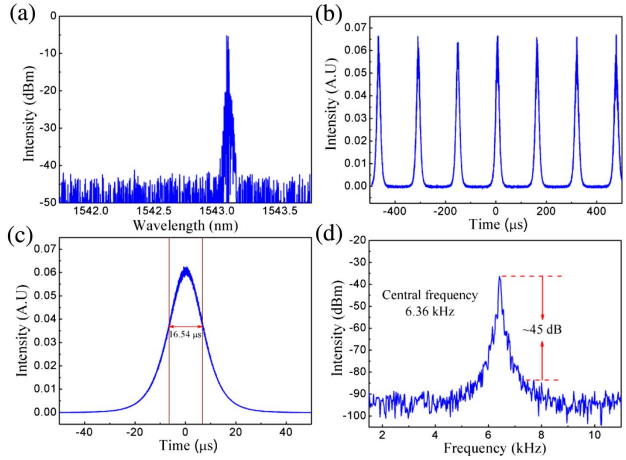

Fig. 10. *Q*-switched operation at a single wavelength of 1543.2 nm. (a) Output optical spectrum, (b) typical *Q*-switched pulse train, (c) single pulse envelope, (d) the RF spectrum.

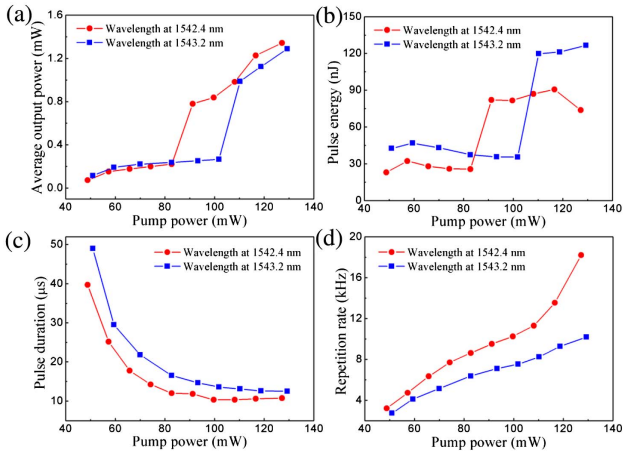

Fig. 11. Single-wavelength Q-switched operation. (a) The average output power, (b) pulse energy, (c) pulse duration, and (d) repetition rate at the wavelengths 1542.4 nm and 1543.2 nm versus pump power.

To compare the pulse characteristics operating at each wavelength, Fig. 11 summarizes their performance versus the pump power. As shown in Figs. 11(a), 11(b), and 11(d), respectively, when the pump power varies from 50 to 130 mW, the average output power increases from 0.1 to 1.4 mW at 1542.4 nm and from 0.15 to 1.35 mW at 1543.2 nm; the pulse energy increases from 15 to 90 nJ at 1542.4 nm and from 45 to 135 nJ at 1543.2 nm; and the repetition rate rises from 3 to 18.5 kHz at 1542.4 nm and from 2.6 to 9.4 kHz at 1543.2 nm. Correspondingly, the pulse duration decreases from 40 to 10 μs at 1542.4 nm and from 50 to 12 μs at 1543.2 nm, as shown in Fig. 11(c). All of them match our theoretical predictions well. The pulse duration curves show some differences between the two wavelengths, mainly due to the different cavity lengths. And the repetition rates at 1542.4 nm are all significantly larger than those at 1543.2 nm, but they are almost in synchrony at the dual-wavelength operation state.

4. CONCLUSIONS

In conclusion, a switchable dual-wavelengths Q-switched EDF ring laser is experimentally realized using a BCM SA. To alleviate the thermal load and ensure the effect of the light–matter interaction, few-layer BP flakes are deposited on a microfiber to fabricate an SA. By the aid of the BCM together with two fiber Bragg gratings, a switchable dual-wavelengths Q-switched fiber laser has been realized at 1542.4 nm and 1543.2 nm (with spacing as small as 0.8 nm). The laser can operate at both dual- and single-wavelength Q-switched laser states, which can be flexibly switched by adjusting the PC carefully. Our results suggest that a BCM SA combined with fiber Bragg gratings may be a good candidate for multiwavelength fiber lasers. When operating at the dual-wavelength state, to further improve the two wavelengths, the laser may be applied to effectively generating a signal at 0.1 THz, indicating its potential applications in terahertz generation. In addition, our dual-wavelength Q-switched fiber laser can also be applied to laser radar [38].

Funding. National Natural Science Foundation of China (NSFC) (61490710, 61505122, 61775142); Science and Technology Planning Project of Guangdong Province (2016B050501005); Specialized Research Fund for the Shenzhen Strategic Emerging Industries Development (JCYJ20170412105812811); Natural Science Foundation of SZU (2017018).

†These authors contributed equally to this work.

REFERENCES

1. U. Keller, "Recent developments in compact ultrafast lasers," Nature **424**, 831–838 (2003).
2. H. Zhang, D. Y. Tang, X. Wu, and L. M. Zhao, "Multi-wavelength dissipative soliton operation of an erbium-doped fiber laser," Opt. Express **17**, 12692–12697 (2009).
3. G. F. Shen, X. M. Zhang, H. Chi, and X. F. Jin, "Microwave/millimeter-wave generation using multi-wavelength photonic crystal fiber Brillouin laser," Prog. Electromagn. Res. **80**, 307–320 (2008).
4. Y. Chen, J. Yin, H. Chen, J. Wang, P. Yan, and S. Ruan, "Single-wavelength and multiwavelength Q-switched fiber laser using Fe_3O_4 nanoparticles," IEEE Photon. J. **9**, 1501009 (2017).
5. M. Wu, S. Chen, Y. Chen, and Y. Li, "Wavelength switchable graphene Q-switched fiber laser with cascaded fiber Bragg gratings," Opt. Commun. **368**, 81–85 (2016).
6. L. Xia, P. Shum, J. Zhou, and T. H. Cheng, "Eight-wavelength switchable fiber ring laser with ultranarrow wavelength spacing using a quadruple-transmission-band polarization maintaining fiber Bragg grating," Appl. Phys. B **88**, 185–188 (2007).
7. S. P. Reilly, S. W. James, and R. P. Tatam, "Tunable and switchable dual wavelength lasers using optical fiber Bragg grating external cavities," Electron. Lett. **38**, 1033–1034 (2002).
8. S. Pan, C. Lou, and Y. Gao, "Multiwavelength erbium-doped fiber laser based on inhomogeneous loss mechanism by use of a highly nonlinear fiber and a Fabry-Perot filter," Opt. Express **14**, 1113–1118 (2006).
9. Y. Lian, G. Ren, B. Zhu, Y. Gao, W. Jian, W. Ren, and S. Jian, "Switchable multiwavelength fiber laser using erbium-doped twin-core fiber and nonlinear polarization rotation," Laser Phys. Lett. **14**, 055101 (2017).
10. S. Yamashita and K. Hotate, "Multiwavelength erbium-doped fiber laser using intracavity etalon and cooled by liquid nitrogen," Electron. Lett. **32**, 1298–1299 (1996).
11. Y. G. Han, T. V. A. Tran, and S. B. Lee, "Wavelength-spacing tunable multiwavelength erbium-doped fiber laser based on four-wave mixing of dispersion-shifted fiber," Opt. Lett. **31**, 697–699 (2006).
12. Z. Luo, M. Zhou, D. Wu, C. Ye, J. Weng, and J. Dong, "Graphene-induced nonlinear four-wave-mixing and its application to multiwavelength Q-switched rare-earth-doped fiber lasers," J. Lightwave Technol. **29**, 2732–2739 (2011).
13. T. Gu, N. Petrone, J. F. McMillan, A. van der Zande, M. Yu, G. Q. Lo, D. L. Kwong, J. Hone, and C. W. Wong, "Regenerative oscillation and four-wave mixing in graphene optoelectronics," Nat. Photonics **6**, 554–559 (2012).
14. Z. Sun, T. Hasan, F. Torrisi, D. Popa, G. Privitera, F. Wang, F. Bonaccorso, D. M. Basko, and A. C. Ferrari, "Graphene mode-locked ultrafast laser," ACS Nano **4**, 803–810 (2010).
15. S. Kumar, M. Anija, N. Kamaraju, K. S. Vasu, K. S. Subrahmanyam, A. K. Sood, and C. N. R. Rao, "Femtosecond carrier dynamics and saturable absorption in graphene suspensions," Appl. Phys. Lett. **95**, 191911 (2009).
16. J. Wang, Y. Hernandez, M. Lotya, J. N. Coleman, and W. J. Blau, "Broadband nonlinear optical response of graphene dispersions," Adv. Mater. **21**, 2430–2435 (2009).
17. Q. Bao, H. Zhang, Y. Wang, Z. Ni, Y. Yan, Z. X. Shen, K. P. Loh, and D. Y. Tang, "Atomic-layer graphene as a saturable absorber for ultrafast pulsed lasers," Adv. Funct. Mater. **19**, 3077–3083 (2009).

18. S. Chen, C. Zhao, Y. Li, H. Huang, S. Lu, H. Zhang, and S. Wen, "Broadband optical and microwave nonlinear response in topological insulator," Opt. Mater. Express **4**, 587–596 (2014).
19. S. Chen, Y. Chen, M. Wu, Y. Li, C. Zhao, and S. Wen, "Stable *Q*-switched erbium-doped fiber laser based on topological insulator covered microfiber," IEEE Photon. Technol. Lett. **26**, 987–990 (2014).
20. Y. Zhao, X. Li, M. Xu, H. Yu, Y. Wu, Z. Wang, X. Hao, and X. Xu, "Dual-wavelength synchronously *Q*-switched solid-state laser with multi-layered graphene as saturable absorber," Opt. Express **21**, 3516–3522 (2013).
21. N. Zhao, M. Liu, H. Liu, X. W. Zheng, Q. Y. Ning, A. P. Luo, Z. C. Luo, and W. C. Xu, "Dual-wavelength rectangular pulse Yb-doped fiber laser using a microfiber-based graphene saturable absorber," Opt. Express **22**, 10906–10913 (2014).
22. Z. Luo, Y. Huang, J. Wang, H. Cheng, Z. Cai, and C. Ye, "Multiwavelength dissipative-soliton generation in Yb-fiber laser using graphene-deposited fiber-taper," IEEE Photon. Technol. Lett. **24**, 1539–1542 (2012).
23. L. Meng, N. Zhao, H. Liu, X. W. Zheng, A. P. Luo, Z. C. Luo, W. C. Xu, C. J. Zhao, H. Zhang, and S. C. Wen, "Dual-wavelength harmonically mode-locked fiber laser with topological insulator saturable absorber," IEEE Photon. Technol. Lett. **26**, 983–986 (2014).
24. B. Guo, Y. Yao, Y. F. Yang, Y. J. Yuan, R. L. Wang, S. G. Wang, Z. H. Ren, and B. Yan, "Topological insulator: Bi_2Se_3/polyvinyl alcohol film-assisted multi-wavelength ultrafast erbium-doped fiber laser," J. Appl. Phys. **117**, 063108 (2015).
25. F. Q. Jia, H. Chen, P. Liu, Y. Huang, and Z. Luo, "Nanosecond-pulsed, dual-wavelength passively *Q*-Switched c-cut Nd:YVO_4 laser using a few-layer Bi_2Se_3 saturable absorber," IEEE J. Sel. Top. Quantum Electron. **21**, 369–374 (2015).
26. H. Zhang, S. Virally, Q. Bao, L. K. Ping, S. Massar, N. Godbout, and P. Kockaert, "Z-scan measurement of the nonlinear refractive index of graphene," Opt. Lett. **37**, 1856–1858 (2012).
27. S. Lu, C. Zhao, Y. Zou, S. Chen, and Y. Chen, "Third order nonlinear optical property of Bi_2Se_3," Opt. Express **21**, 2072–2082 (2013).
28. F. D. Muhammad, M. Z. Zulkifli, A. A. Latif, S. W. Harun, and H. Ahmad, "Graphene-based saturable absorber for single-longitudinal-mode operation of highly doped erbium-doped fiber laser," IEEE Photon. J. **4**, 467–475 (2012).
29. H. Ahmad, F. D. B. Muhammad, M. Z. Zulkifli, A. A. Latif, and S. W. Harun, "Tunable radio frequency generation using a graphene-based single longitudinal mode fiber laser," J. Lightwave Technol. **30**, 2097–2102 (2012).
30. L. Lu, X. Tang, R. Cao, L. Wu, Z. Li, G. Jing, B. Dong, S. Lu, Y. Li, Y. Xiang, J. Li, D. Fan, and H. Zhang, "Broadband nonlinear optical response in few-layer antimonene and antimonene quantum dots: a promising optical Kerr media with enhanced stability," Adv. Opt. Mater. **5**, 1700301 (2017).
31. T. Low, A. S. Rodin, A. Carvalho, Y. Jiang, H. Wang, F. Xia, and A. H. C. Neto, "Tunable optical properties of multilayer black phosphorus thin films," Phys. Rev. B **90**, 075434 (2014).
32. Y. Xu, W. Wang, Y. Ge, H. Guo, X. Zhang, S. Chen, Y. Deng, Z. Lu, and H. Zhang, "Stabilization of black phosphorous quantum dots in PMMA nanofiber film and broadband nonlinear optics and ultrafast photonics application," Adv. Funct. Mater. **27**, 1702437 (2017).
33. D. Li, H. Jussila, L. Karvonen, G. Ye, H. Lipsanen, X. Chen, and Z. Sun, "Polarization and thickness dependent absorption properties of black phosphorus: new saturable absorber for ultrafast pulse generation," Sci. Rep. **5**, 15899 (2015).
34. J. Zheng, X. Tang, Z. Yang, Z. Liang, Y. Chen, K. Wang, Y. Song, Y. Zhang, J. Ji, Y. Liu, D. Fan, and H. Zhang, "Optical modulation: few-layer phosphorene-decorated microfiber for all-optical thresholding and optical modulation," Adv. Opt. Mater. **5**, 1700026 (2017).
35. J. Zheng, Z. Yang, C. Si, Z. Liang, X. Chen, R. Cao, and M. Zhang, "Black phosphorus based all-optical-signal-processing: towards high performances and enhanced stability," ACS Photon. **4**, 1466–1476 (2017).
36. Y. Chen, S. Chen, J. Liu, Y. Gao, and W. Zhang, "Sub-300 femtosecond soliton tunable fiber laser with all-anomalous dispersion passively mode locked by black phosphorus," Opt. Express **24**, 13316–13324 (2016).
37. S. B. Lu, L. L. Miao, Z. N. Guo, X. Qi, C. J. Zhao, H. Zhang, S. C. Wen, D. Y. Tang, and D. Y. Fan, "Broadband nonlinear optical response in multi-layer black phosphorus: an emerging infrared and mid-infrared optical material," Opt. Express **23**, 11183–11194 (2015).
38. B. Lashkari, S. S. S. Choi, M. E. Khosroshahi, E. Dovlo, and A. Mandelis, "Simultaneous dual-wavelength photoacoustic radar imaging using waveform engineering with mismatched frequency modulated excitation," Opt. Lett. **40**, 1145–1148 (2015).